Journal of Physics: Conference Series **154** (2009) 012006 doi:10.1088/1742-6596/154/1/012006

Phase noise contribution of EOMs and HF cables

Simon Barke, Michael Tröbs, Benjamin Sheard, Gerhard Heinzel, Karsten Danzmann

Max Planck Institute for Gravitational Physics, Callinstr. 38, 30167 Hannover, Germany

E-mail: simon.barke@aei.mpg.de

Abstract. Two key components of LISA's inter-spacecraft clock tone transfer chain are electro-optic modulators (EOMs) and high-frequency (HF) cable assemblies. At modulation frequencies of 2 GHz, we characterized the excess phase noise of these components in the LISA frequency range (0.1 mHz to 1 Hz). The upper phase noise limit was found to be almost an order of magnitude better than required. In addition, phase dependencies on temperature were determined. The measured coefficients are within a few milliradians per Kelvin and thereby negligible due to the specified on-board temperature stability.

1. Introduction

The total setup phase noise detected by the LISA phasemeter must not exceed an equivalent spacecraft displacement of $1\,\frac{\mathrm{pm}}{\sqrt{\mathrm{Hz}}}$ [1, 2]. This translates to a phase noise requirement of $\Delta\phi_{1\mathrm{pm}} < 6\,\frac{\mu\mathrm{rad}}{\sqrt{\mathrm{Hz}}}$. To reach this 1 pm requirement, an inter-spacecraft clock tone transfer chain is necessary to remove the non-negligible ultra-stable oscillator (USO) phase noise. In the current baseline design, the signal generated by the on-board USOs is up-converted, and superimposed by EOMs on each of the six laser beams (Fig. 1, left) [3, 4]. The main carrier signal is then transmitted, together with the modulation sidebands, to the receiving spacecraft (Fig. 1, right). Here they are heterodyned with a local laser beam. A photodiode now detects three beat notes: The carrier-carrier beat at a frequency up to 20 MHz and the two sideband-sideband beats. Since the sidebands were imposed onto the laser beams by a signal phase locked to the USO signal, the sideband-sideband beat notes contain information about the USO phase noises. Using this information the USO noise can be removed to acceptable levels [5].

1.1. The ancillary modulation error

The components of the clock transfer chain might add excess phase noise to the sidebands which is referred to as ancillary modulation error (AME). To obtain a modulation frequency $f_{\mathrm{mod}} \approx 2\,\mathrm{GHz}$, one multiplies the USO frequency $f_{\mathrm{USO}} \approx 80\,\mathrm{MHz}$ by the factor $\frac{f_{\mathrm{mod}}}{f_{\mathrm{USO}}}$, while the ADC is triggered directly by the USO. The magnitude of a phase shift in a signal being up-converted by a frequency multiplier is increased linearly by the multiplication factor [6]. Therefore—with respect to the design sensitivity—one can derive an AME requirement of

$$\Delta\phi_{\mathrm{AME}} < \Delta\phi_{1\mathrm{pm}}\frac{f_{\mathrm{USO}}\cdot f_{\mathrm{mod}}}{f_{\mathrm{het}}\cdot f_{\mathrm{USO}}}\sqrt{1+\left(\frac{2.8\cdot 10^{-3}\,\mathrm{Hz}}{f}\right)^4} \approx 0.6\cdot\sqrt{1+\left(\frac{2.8\cdot 10^{-3}\,\mathrm{Hz}}{f}\right)^4}\,\frac{\mathrm{mrad}}{\sqrt{\mathrm{Hz}}}, \quad (1)$$

which increases as $1/f^2$ for frequencies below 2.8 mHz and is valid in the LISA frequency range.

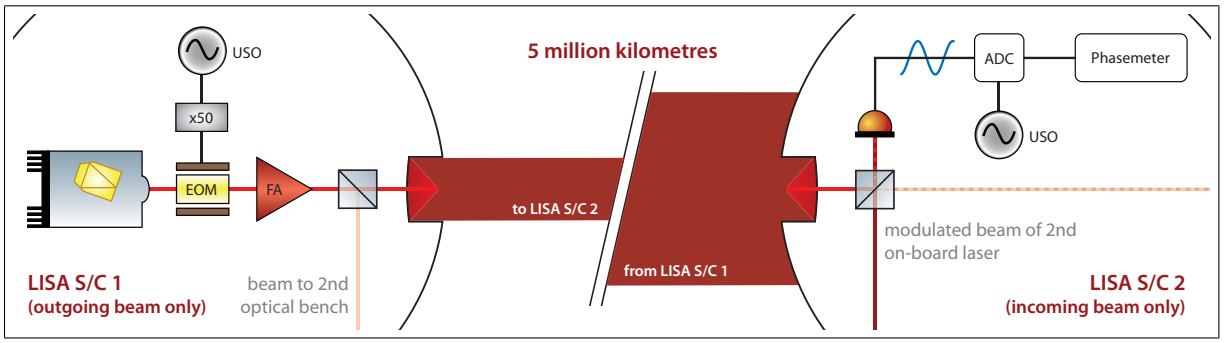

Figure 1. Inter-spacecraft clock transfer scheme: outgoing beam (left), incoming beam (right).

1.2. Phase characteristics of transfer chain components
Experiments are essential to characterize suitable components and to find devices phase stable enough to be used for the clock tone transfer chain. This paper presents measurements of the AME induced during the modulation process by the EOM or HF cable assemblies. EOM phase characteristics were investigated recently, but only for pairs of EOMs (differential processing of sideband pairs) and at modulation frequencies of 8 GHz [7]. The advantages of such high modulation frequencies are: (i) less sideband power is needed in order for clock calibration noise to be $\frac{1}{10}$ of the carrier-carrier shot-noise limit [8], and (ii) the relaxation upon the phase stability requirements is higher. The disadvantages, however, are a higher electrical power necessary for generating sidebands at higher frequencies and all common problems involved with HF electronics. We aim for a lower sideband frequency as proposed by [9].

2. Electro-optic modulator
For our sideband phase stability research we used a *Fibre-coupled Integrated Optical Phase Modulator* by Jenoptik. This EOM is polarization-maintaining and allows broadband phase modulation for frequencies up to 3 GHz. The electro-optic medium used is a waveguide made of magnesium oxide doped lithium niobate ($MgO:LiNbO_3$) which provides a high damage threshold. Single-mode fibres with FC/APC connectors are used to couple the light in and out with a typical overall insertion loss of 4 dB. The spectral bandwidth is specified as 1064 ± 60 nm. By connecting the EOM output to a fibre-coupled confocal scanning Fabry-Perot interferometer, we determined the modulation efficiency at a modulation frequency (f_{mod}) of $\sim$2 GHz to be 0.37 $\frac{\mathrm{rad}}{\mathrm{V}}$ which is equivalent to a half-wave voltage (the voltage necessary for a modulation index of $m = \pi$) of 8.6 V.

2.1. Potential phase noise sources
There are several effects in the ferroelectric substrate of the optical waveguides used in integrated EOMs which might add excess phase noise to the sidebands. A heat-induced expansion will change the length of the waveguide and thereby the optical path length, which leads to an unwanted phase shift. In addition, expansion of the waveguide substrate may lead to stress. The waveguide's refractive index is not constant over temperature which is also referred to as the thermo-optic effect. Due to the material's pyroelectricity, changes in temperature can also produce an electric potential (pyroelectric effect). This potential will then shift the phase of the light due to the linear electro-optic effect (Pockels effect) of lithium niobate [10]. Furthermore, for lithium niobate the refractive index decreases in response to higher optical powers which is referred to as the photorefractive effect [11].

2.2. Measurement setup

Fig. 2 shows a schematic of the setup used to measure the phase noise of a single EOM sideband. Two lasers at 1064 nm (L1 and L2) were offset phase locked to $f_{\mathrm{Ref}} = 2\,\mathrm{GHz} + 1.6\,\mathrm{kHz}$ with one beam (L1) sent through the EOM under test driven by a signal at $f_{\mathrm{Mod}} = 2\,\mathrm{GHz}$. We obtained a signal level of 18 dBm driving the EOM. This resulted in a modulation index of $m = 0.65$ or respectively 12% of the carrier power in a single sideband. Both laser beams were heterodyned at a beamsplitter and sent to a photodiode where different heterodyne frequencies were detected: the two carriers beating against each other; and the two sidebands of laser L1 beat against the carrier of laser L2. In a simplified description avoiding the spatial mode and polarization of the electrical fields, the two dectectable beat notes within the photodetector bandwith are: (i) for the carrier-carrier signal at 2 GHz+1.6 kHz

$$U_{\mathrm{HF}} \propto A_{\mathrm{L1}} J_0\left(m\right) A_{\mathrm{L2}} \cdot \cos\left(2\pi f_{\mathrm{Ref}} t\right), \tag{2}$$

and (ii) for the sideband-carrier signal at 1.6 kHz

$$U_{\mathrm{LF}} \propto A_{\mathrm{L1}} J_1\left(m\right) A_{\mathrm{L2}} \cdot \cos\left[2\pi\left(f_{\mathrm{Ref}} - f_{\mathrm{Mod}}\right) t - \phi_{\mathrm{EOM-}}\left(t\right)\right], \tag{3}$$

where $\phi_{\mathrm{EOM-}}\left(t\right)$ is the phase noise of the lower sideband. A_{L1} and A_{L2} are the electrical field amplitudes of the two laser beams (L1 and L2), m is the modulation index which is proportional to the amplitude of the signal driving the EOM ($m \propto A_{\mathrm{Mod}}$) and $J_n\left(m\right)$ is the Bessel function of the first kind, order n, for the value m. Since for the EOM phase characterization we used a low modulation index of $m \approx 0.6$ one can ignore the higher-order sidebands.

The carrier-carrier beat note (Eq. (2)) was passed to an electronic mixer and mixed down with the same signal driving the EOM. Considering only the low-pass filtered signal of the mixer output we thereby obtained another signal at 1.6 kHz:

$$U_{\mathrm{Mix}} \propto \frac{A_{\mathrm{L1}} J_0\left(m\right) A_{\mathrm{L2}} A_{\mathrm{Mod}}}{2} \cdot \cos\left[2\pi\left(f_{\mathrm{Ref}} - f_{\mathrm{Mod}}\right) t\right]. \tag{4}$$

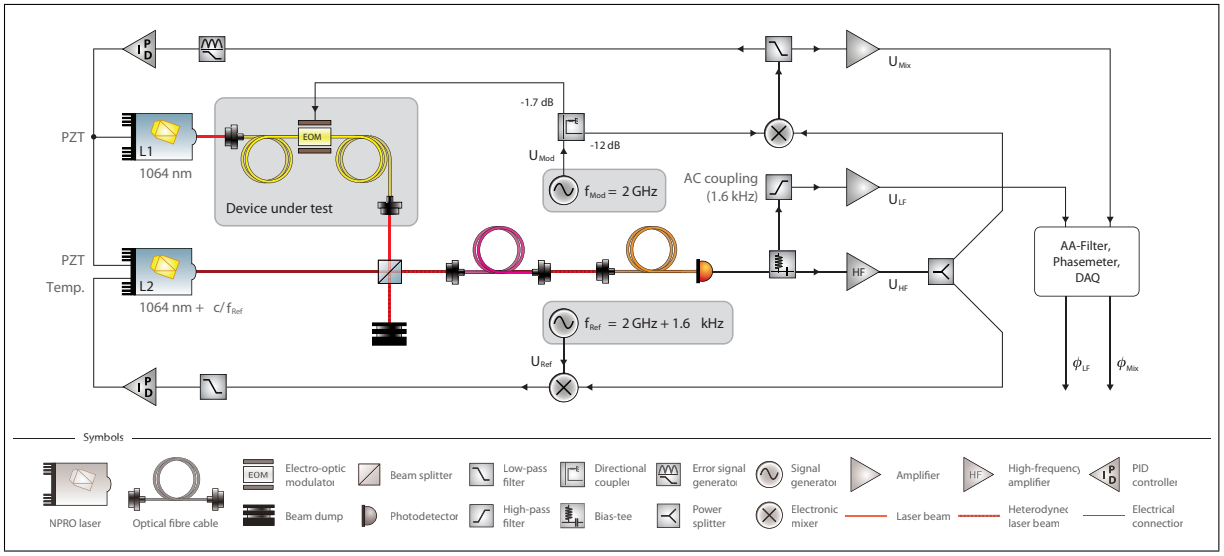

Figure 2. Setup for measuring the phase characteristics of a single EOM sideband at 2 GHz (schematic): Two lasers (one modulated by an EOM at $f_{\mathrm{Mod}} = 2\,\mathrm{GHz}$) offset phase locked to $f_{\mathrm{Ref}} = 2\,\mathrm{GHz} + 1.6\,\mathrm{kHz}$ were heterodyned and power stabilized with respect the amplitude of the 2 GHz beat note by a second control loop.

A DC voltage proportional to the amplitude of the U_{Mix} signal was passed to a loop filter which was connected to both laser diode current drivers. Hence we were able to stabilize the beat note power. The EOM phase noise measurement required the phase information of the two signals described by Eq. (3) and Eq. (4). A software phasemeter operating with the same principle as the LISA Technology Package (LTP) phasemeter was used for this purpose [12]. After determining the phase of both signals (where ϕ_{Mix} is the phase of U_{Mix} and ϕ_{LF} is the phase of U_{LF}) we calculated the differential phase $\Delta\phi = \phi_{\mathrm{Mix}} - \phi_{\mathrm{LF}}$. The spectral phase noise densities of the differential phases were then calculated by the LPSD program [13].

One finds that the phase noise of the lower EOM sideband ($\phi_{\mathrm{EOM}-}(t)$) is observable in the differential phase $\Delta\phi$. Further phase noise induced by the frequency generators and the phase-locked loop (PLL) electronics are common-mode and thereby cancel in the differential phase. However, noise induced by cables, photodiodes, HF electronics and the EOM itself is not common-mode and therefore visible in the differential phase $\Delta\phi$. Thus all HF electronics, the lasers, optics and the EOM were isolated by extruded polystyrene boxes providing a low thermal conductivity of $0.03\,\frac{\mathrm{W}}{\mathrm{m\cdot K}}$ and thereby a temperature stability of about $0.1\,\frac{\mathrm{K}}{\mathrm{Hz}}$ at $10^{-3}\,\mathrm{Hz}$. Still the spectral phase noise density, calculated from a time series of $\Delta\phi$, represents an upper limit for the sideband phase noise induced by the EOM under test.

2.3. Measurement results

Fig. 3 shows the phase noise calculated from a time series of $\Delta\phi$ recorded over several hours. The upper limit of the EOM's phase noise (red solid curve) was better than the requirements over the whole frequency range. For comparison a measurement without amplitude stabilization is shown (red dashed curve). Here signal power fluctuations increased the phase noise by about an order of magnitude. The phasemeter sensitivity (blue curve) was well within the required level.

To measure the phase shift caused by a change in the EOM temperature, we constructed a two-part aluminium housing for the EOM with Peltier elements and a heat sink mounted on top. We then intentionally varied the EOM temperature in a range between 22 and 25 °C. Multiple temperature sensors were installed in the top and bottom parts. Fig. 4 shows a plot of the phase shift induced by the EOM versus its temperature. The measurement data is highlighted in red for the warming periods and in orange for the cooling periods. A linear fit is shown in blue which presents a correlation of $2.05 \pm 0.03\,\frac{\mathrm{mrad}}{\mathrm{K}}$.

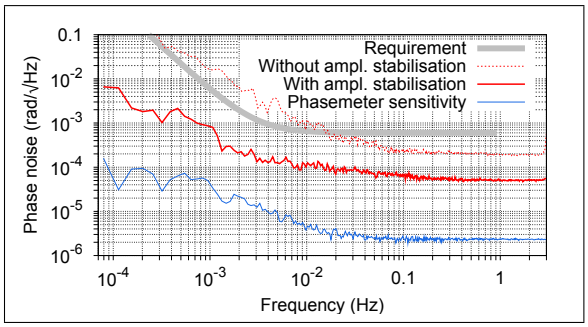

Figure 3. Upper Jenoptik EOM spectral phase noise density limit at 2 GHz modulation frequency.

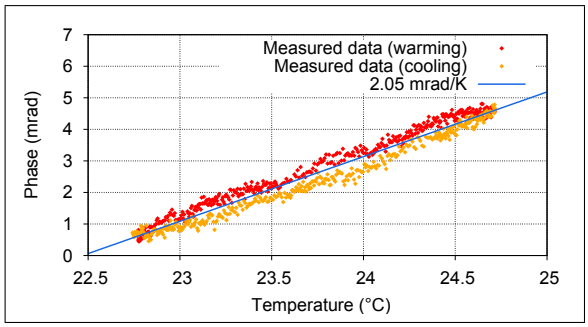

Figure 4. Differential phase versus EOM temperature measurement on Jenoptik EOM at 2 GHz modulation frequency.

3. HF cable assembly

In the EOM phase characteristics measurements discussed above, one cannot distinguish between EOM sideband phase noise added by the HF cable due to changes in temperature and the noise added by the EOM itself. Hence one needs to be sure that the cable is not adding a significant level of excess phase noise to a signal in the region of interest. In the following we concentrate on one representative cable assembly, a 1.22 m long micro-porous *Teflon* (PTFE) dielectric cable named *minibend LR* from Astrolab, USA. Its frequency range is up to 26.5 GHz with an attenuation of 0.93 $^{\mathrm{dB}}/_{\mathrm{m}}$ at 2 GHz.

3.1. Measurement setup

To measure the temperature-induced phase shift of a 2 GHz signal in an electrical cable, a split 2 GHz signal was sent through two identical cables and passed to mixers, each connected to a split 2 GHz + 1.6 kHz signal. Since the mixing process preserves any original phase shifts of the high-frequency signals, the low-pass filtered output of each mixer provided the phase information of the corresponding signal line and was sent to a phasemeter. The setup was divided into two parts. Each part was thermally isolated with an extruded polystyrene box. The first part, which contained the reference cable and all HF electronics, was kept at a constant temperature, while the temperature of the second part, which contained part of the cable under test, was periodically altered by a heating tape, connected to a remotely controlled power supply to alter the temperature of the cable under test between 25 and 45 °C.

3.2. Measurement results

Fig. 5 shows that the temperature-induced phase shift is not linear. Between 25 and 35 °C we observed a maximum slope of $1.2 \pm 0.2\ \frac{\mathrm{mrad}}{\mathrm{K \cdot m}}$. Between 35 and 45 °C the cable is much more phase stable with a maximum slope of $0.2 \pm 0.2\ \frac{\mathrm{mrad}}{\mathrm{K \cdot m}}$. Early measurements performed over a wider temperature range (tendential behaviour in Fig. 5, dashed curve) indicated a rapid phase shift at room temperature which is referred to as the *Teflon* knee [14].

The cable's long time phase noise is presented in Fig. 6. The blue curve shows the phasemeter sensitivity which is well within the phase stability requirement for 2 GHz shown in grey. The red curve represents the phase characteristics of the cable under test while it was exposed to laboratory's temperature fluctuations, while the orange curve is the phase noise when both cables were kept inside the thermal isolation box. The phase noise induced by the cable under test was in both cases better than the requirements.

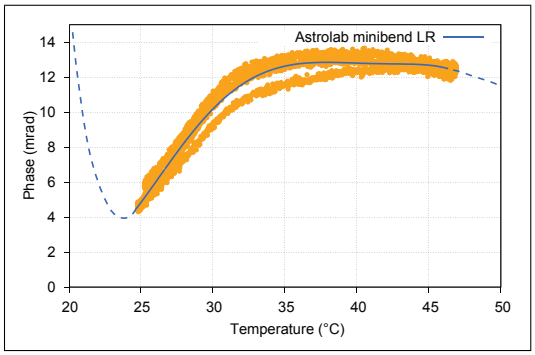

Figure 5. Differential phase versus temperature measurement for an Astrolab *minibend LR* cable, scaled to 1 m length.

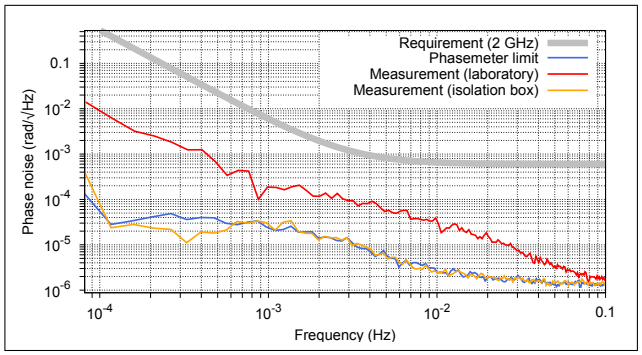

Figure 6. Spectral phase noise densities for an Astrolab *minibend LR* cable with and without thermal isolation box, scaled to 1 m length.

4. Conclusions

We reported on the sideband phase characteristics of a Jenoptik fibre-coupled integrated EOM at modulation frequencies of 2 GHz in the LISA frequency range (1 mHz to 1 Hz). The upper phase noise limit was almost an order of magnitude better than the required 0.6 $\frac{\text{mrad}}{\sqrt{\text{Hz}}}$. The EOM's phase dependence on its temperature was measured to be $2.05 \pm 0.03 \, \frac{\text{mrad}}{\text{K}}$. The designed temperature stability for LISA is $9.1 \cdot 10^{-8} \, \frac{\text{K}}{\sqrt{\text{Hz}}}$ at the optical bench and $10^{-5} \, \frac{\text{K}}{\sqrt{\text{Hz}}}$ at the gravity reference sensor (GRS) housing with an absolute temperature of 293 K [2]. Therefore, the given stability easily guarantees that the EOM fulfils the phase stability requirements with a large margin. One now needs to identify a space qualified version providing an equivalent performance.

Furthermore we showed that the phase noise induced to a 2 GHz signal by a representative HF cable—even when exposed to laboratory's temperature fluctuations—was well within the requirements. In addition, insight into the continuous dependency between temperature and phase of the HF cable under test was presented and we are about to perform measurements with a wider temperature range to map the phase unstable area around room temperature (*Teflon* knee).

Acknowledgments

We gratefully acknowledge support by Deutsches Zentrum für Luft- und Raumfahrt (DLR) (reference 50 OQ 0601).

References

[1] Faulks H et al 2000 *Study of the Laser Interferometer Space Antenna, Final Technical Report* (European Space Research and Technology Center)
[2] EADS Astrium 2007 personal communication
[3] LISA Study Team 1998 *LISA. Laser Interferometer Space Antenna for the detection and observation of gravitational waves. An international project in the field of Fundamental Physics in Space. Pre-Phase A report* (Garching, Germany: Max-Planck-Institut für Quantenoptik)
[4] Hellings R W 2001 *Phys. Rev. D* **64** 022002
[5] Tinto M et al 2002 *Phys. Rev. D* **65** 082003
[6] Couch II L W 1990 *Digital and Analog Communications Systems* (New York: Macmillan)
[7] Klipstein W et al 2006 *Laser Interferometer Space Antenna: 6th International LISA Symposium* (*American Institute of Physics Conference Series* vol 873) ed Merkovitz S M and Livas J C pp 312–318
[8] Folkner W et al 2004 *Presentation at the 5th International LISA Symposium*
[9] Tinto M et al 2008 *Classical and Quantum Gravity* **25** 015008 (12pp)
[10] Ruske J P 2004 *Integriert-optische Bauelementekonzepte zur Führung und Beeinflussung von Licht hoher Leistung und Photonenenergie* Habilitation thesis Friedrich-Schiller-Universität Jena Germany
[11] Steinberg S 1994 *Experimentelle Untersuchung optischer Phaseninstabilitäten an Streifenwellenleitern und elektrooptischen Phasenmodulatoren in LiNbO3 unter besonderer Berücksichtigung des Protonenaustausches* Ph.D. thesis Friedrich-Schiller-Universität Jena Germany
[12] Heinzel G et al 2004 *Classical and Quantum Gravity* **21** S581–S587
[13] Tröbs M et al 2006 *Measurement* **39** 120–129
[14] Micro Coax Application Notes 27 *Understanding Phase Versus Temperature Behavior: The Teflon Knee.*